

Accepted Manuscript

Residual Stress Distribution in a Functionally Graded Alumina-Silicon Carbide Material

C.E.J. Dancer, M. Achintha, C.J. Salter, J.A. Fernie, R.I. Todd

PII: S1359-6462(12)00306-5

DOI: <http://dx.doi.org/10.1016/j.scriptamat.2012.05.002>

Reference: SMM 9410

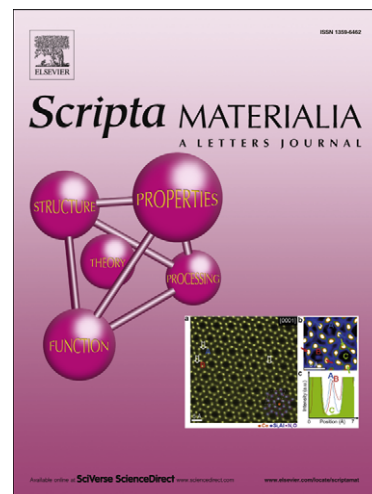
To appear in: *Scripta Materialia*

Received Date: 26 March 2012

Accepted Date: 1 May 2012

Please cite this article as: C.E.J. Dancer, M. Achintha, C.J. Salter, J.A. Fernie, R.I. Todd, Residual Stress Distribution in a Functionally Graded Alumina-Silicon Carbide Material, *Scripta Materialia* (2012), doi: <http://dx.doi.org/10.1016/j.scriptamat.2012.05.002>

This is a PDF file of an unedited manuscript that has been accepted for publication. As a service to our customers we are providing this early version of the manuscript. The manuscript will undergo copyediting, typesetting, and review of the resulting proof before it is published in its final form. Please note that during the production process errors may be discovered which could affect the content, and all legal disclaimers that apply to the journal pertain.



Residual Stress Distribution in a Functionally Graded Alumina-Silicon Carbide Material

C.E.J. Dancer^{1*}, M. Achintha², C.J. Salter¹, J.A. Fernie^{1,3} and R.I. Todd¹

¹ Department of Materials, University of Oxford, Parks Road, Oxford, OX1 3PH, UK

² Department of Engineering Science, University of Oxford, Parks Road, Oxford, OX1 3PJ, UK

³ Ceramics Joining Limited, Tidmarsh House, Tidmarsh, Reading, RG8 8HA

* Corresponding author. Email: claire.dancer@materials.ox.ac.uk

Abstract

Functionally graded ceramic structures have a range of potential applications as they enable the exploitation of two ceramic materials with very different properties, such as coefficient of thermal expansion. We report the microstructural investigation of a novel functionally graded structure for alumina and silicon carbide with systematically varied composition. Stresses in the structure have been modelled analytically and by finite element modelling, and are consistent with fluorescence microscopy measurements of residual stress in the structure.

Keywords

Functionally Graded Materials; Ceramics; Residual Stresses.

Functionally graded materials (FGMs) possess a systematically varied microstructure and/or composition resulting in gradual changes in their mechanical, physical and/or chemical properties across the geometry [1]. FGMs have been proposed as an interlayer for joining dissimilar materials (both ceramic-ceramic and ceramic-metal couples), as they potentially reduce the residual stresses caused by the mismatch in coefficients of thermal expansion (CTE) [2,3] and the large temperature changes in the manufacturing process.

In this work we investigate the microstructure in a ceramic FGM cylinder with composition which changes semi-continuously from SiC-rich at one end to Al₂O₃-rich at the other. By this we mean that the FGM is made up of individual layers with each adjacent layer having a slightly different composition such that at one end it is predominantly SiC, and at the other predominantly Al₂O₃. The CTEs of SiC and Al₂O₃ are significantly different at $4.7 \times 10^{-6} \text{ } ^\circ\text{C}^{-1}$ for SiC (for temperatures 0-1700°C) and $8.6 \times 10^{-6} \text{ } ^\circ\text{C}^{-1}$ for Al₂O₃ (for 0-1727°C) [4]. The number and thickness of the individual layers must be chosen to keep the generated residual stresses within acceptable limits and so avoid cracking. We then use experimental measurements along with finite element and analytical models to determine the residual stresses developed in the cylinder.

The production of slab-like SiC/C ceramic FGMs [5] and Al₂O₃-Si₃N₄ graded structures [6] have previously been reported, but Al₂O₃-SiC FGMs have not been described before to our knowledge. The cylindrical FGM in our work had diameter and length of 20mm and individual layers in the final structure were approximately 2.2mm thick, which is within the range suggested for ceramic-metal FGM structures of similar dimensions [7]. The layers

1 were assembled using submicron powders mixed in suitable proportions, and hot pressed
2 under uniaxial load at temperatures up to 1800°C in an inert atmosphere.

3 SiC is typically processed using sintering aids consisting of a combination of
4 aluminium, boron and carbon (or compounds of these) [8-10] which lower the sintering
5 temperature to 1850-2100°C, while maintaining good mechanical properties [11]. However
6 for this assembly it is critical that the sintering temperature is below 1850°C in order to
7 prevent excessive grain growth of alumina at the alumina-rich end of the structure. In
8 addition, the integrity of the FGM will be affected by the thermal expansion mismatch
9 between SiC and Al₂O₃, which will become larger if cooling is from higher temperatures.

10 An alternative route is to use a combination of oxide phases as liquid-phase sintering
11 aids [8,12] (“LPS SiC”). The literature shows that the highest density SiC at the lowest
12 sintering temperature was obtained by Sciti and Bellosi using hot pressing, by adding a
13 mixture of 4wt.% Y₂O₃ and 6wt.% Al₂O₃ to 90wt% SiC powder [8] at 1800°C and 30MPa
14 pressure, which had density above 98% of the theoretical maximum. This composition was
15 therefore chosen for the SiC-rich end of the FGM.

16 The processing requirements for densification of monolithic Al₂O₃ are well
17 established [13]. Ultra-high purity Al₂O₃ can be fully densified without abnormal grain
18 growth (AGG) [13,14]. However low levels of MgO is often added to avoid AGG and
19 increase strength [13,15], as AGG caused by slight contamination of the starting powder is
20 common [16]. Dense Al₂O₃ with small grain size can be produced by hot pressing alumina
21 powder with 0.25wt.% MgO in flowing argon at temperatures of 1470-1650°C and under 25
22 MPa uniaxial pressure [17]. However, higher temperatures were required here to fully densify
23 the SiC-rich end of the FGM, which could result in a large grain size and decreased strength
24 at the Al₂O₃-rich end. Therefore, the final layer of the FGM had composition 10wt.% SiC-
25 Al₂O₃.

26 The intermediate layers of this FGM have systematically varying Al₂O₃ and SiC
27 content. Dense SiC-Al₂O₃ composites with up to 30vol.% Al₂O₃ content have been produced
28 by a number of researchers [18-21]. While these compositions are now well-established, we
29 are unaware of any research reported in the literature on the production of Al₂O₃-SiC
30 composites containing 40-80% SiC by powder processing. Yang and Troczynski [22] used
31 sol-gel processing and pressureless sintering to produce Al₂O₃-SiC composites with up to
32 60vol.% SiC content but this method is not completely suitable for the production of FGM
33 structures due to the high shrinkage during processing and relatively high residual porosity
34 [22].

35 The composition used for the SiC-richest layer was modified for 40-80% SiC
36 compositions. In the SiC-richest layer, under appropriate heat-treatment conditions, Y₂O₃ and
37 Al₂O₃ powders form a liquid sintering aid [23]. The presence of YAG was confirmed by X-
38 ray diffraction (not shown) of discs with the SiC-rich compositions. The Y₂O₃ and Al₂O₃
39 contents were linearly decreased from the amount added to the SiC-richest layer to zero for
40 the 30% SiC layer.

41 Fig. 1a shows a typical FGM assembly consisting of 9 layers. The cylinder was
42 sectioned lengthways using a diamond blade, mounted in resin and polished (Fig. 1b).
43 Microstructural analyses were carried out in order to understand the compositional variations
44 and residual stresses within the FGM.
45
46
47
48
49
50
51
52
53
54
55
56
57
58
59
60
61
62
63
64
65

1 Examination of the polished cross-section by optical microscopy revealed no
 2 macroscopic cracking. Some porosity was evident at the boundary between the 80 and 90%
 3 SiC layers. Further investigations were made using a field-emission scanning electron
 4 microscope (JEOL 6500F) in back-scattered mode (Fig. 2). The Al₂O₃-rich end (Fig. 2a)
 5 contains submicron SiC particles (grey) in an Al₂O₃ matrix (lighter) and with limited fine
 6 scale porosity (black). The Al₂O₃ grain size is 3-5µm. The microstructure at the centre of the
 7 rod (Fig. 2b) was similar to the Al₂O₃-rich end, with more SiC and slightly more residual
 8 porosity. The white regions are mainly YAG originating from the liquid phase. Interfaces
 9 were confirmed to be crack-free and relatively sharp.

10 The 80% SiC layer showed unusual “fern-like” features close to the interface with the
 11 90% SiC layer (Fig. 2c) over ~100µm regions orientated approximately perpendicular to the
 12 interface. The strong atomic number contrast of the features indicates that some flow and
 13 segregation of the YAG liquid phase occurred during sintering, possibly driven by capillary
 14 forces resulting from regions of different density. The microstructure within the rest of the
 15 SiC-rich end (Fig. 2d) contains some small inhomogeneous regions. Areas which were richer
 16 in liquid have sintered well and conversely the regions that are deficient in liquid show some
 17 fine scale porosity. Similar segregation has been observed in LPS SiC densified by
 18 FAST/SPS and was attributed to the formation of large YAG crystals during cooling [24].

19 To study the residual stresses in the FGM, fluorescence microscopy experiments were
 20 performed on the cross-section using a confocal Raman microscope (System 1000, Renishaw,
 21 UK) with a motorised stage and incident radiation from a 633 nm He-Ne laser (50x lens,
 22 spatial resolution ~5µm). The position of the R1 fluorescence peak (associated with Cr³⁺
 23 impurities [25]) was measured every 0.25mm along the length of the rod and repeated 3 times
 24 along different lines (Fig. 3). This wavelength is related to the mean stress (σ_m) by Eq. (1),
 25 where $\Delta\nu$ is the change in wavenumber and $\bar{\Pi}_m$ is the mean piezospectroscopic coefficient
 26 (7.59cm⁻¹GPa⁻¹ for polycrystalline alumina) [26].

$$\Delta\nu = \bar{\Pi}_m \sigma_m \quad (1)$$

27 In the 7th layer of the sample (70% SiC) the Al₂O₃/Cr³⁺ fluorescence signal became
 28 too weak to measure accurately owing to the diminishing amount of alumina. However
 29 observations on the alumina-rich end enable us to assess the general trend in the residual
 30 stress. The good agreement between the three separate line scans shows the reproducibility of
 31 the technique and the uniformity of the stresses in the rod.

32 There are two main sources of residual stress in the FGM structure: the thermal
 33 expansion mismatch between Al₂O₃ and SiC in the individual composite layers
 34 (“microstresses”), and the mismatch between the layers. Both contribute to shifts in
 35 fluorescence peak position. At the Al₂O₃-rich end, the microstresses caused by the CTE
 36 mismatch between SiC and Al₂O₃ during cooling can be modelled as an assembly of
 37 spherical SiC particles, each surrounded by a concentric spherical shell of alumina with
 38 radius chosen to give the correct volume fraction of each component. This has been used
 39 previously to understand residual stresses in non-FGM sections of similar composites
 40 [19,27]. The volume-averaged mean stress in the alumina, σ_A , can then be assessed [27]:

1
2
3
4
5
6
7
8
9
10
11
12
13
14
15
16
17
18
19
20
21
22
23
24
25
26
27
28
29
30
31
32
33
34
35
36
37
38
39
40
41
42
43
44
45
46
47
48
49
50
51
52
53
54
55
56
57
58
59
60
61
62
63
64
65

$$\sigma_A = \frac{fE_A E_S (\alpha_A - \alpha_S) \Delta T}{(1-f)E_A (1-2\nu_S) + E_S [f(1-2\nu_A) + \frac{1}{2}(1+\nu_A)]} \quad (2)$$

where subscripts *A* and *S* refer to the alumina and SiC respectively, *E* is Young's modulus, ν is Poisson's ratio, *f* is the volume fraction of SiC, α is linear thermal expansion coefficient, and ΔT is the temperature drop over which the stresses have not been relaxed (*e.g.* by diffusion).

Eq. (2) indicates that the microstresses in the Al₂O₃ are expected to increase as more SiC is added. Using material property data from Todd *et al* [27] and $\bar{\Pi}_m$ as given above allows the predicted peak shift for the microstresses alone to be calculated using Eq.s (1) and (2). Previous work [19, 28] shows that the instrument used mainly samples the bulk stresses in materials such as these where one phase is transparent. These are plotted compared with the fluorescence line scan results (Fig. 3) using the nominal midpoints of the layers on the abscissa. The R1 wavenumber is taken as 14404cm⁻¹ at the centre of the Al₂O₃-richest layer, and the reasonable value of 1000°C was assumed for ΔT . The agreement is good, showing that the large steps in fluorescent wavelength between layers are due primarily to the microstresses, rather than larger stresses due to the FGM layers. Although the microstresses are large (*e.g.* $\sigma_A \sim 800$ MPa in the 50% SiC layer), they do not cause cracking because they act over short distances. Previous work has shown that the addition of SiC particles to Al₂O₃ does not cause cracking until the SiC particles are larger than 10 μ m [20]; these particles are much smaller ($\sim 0.5\mu$ m) than this critical size.

As the steps observed between layers in Fig. 3 are evidently primarily attributable to the difference in interphase microstresses within each layer, the stresses resulting from mismatches between layers of the FGM are expected to be relatively small. The average Cr³⁺ R1 fluorescence peak shift across each layer is 0.24 \pm 0.09cm⁻¹ corresponding to a mean stress of 32 \pm 10MPa from Eq. (1). To examine this further, a commercial FE package (ABAQUS) was also used to determine the distribution of stresses (Fig.4). Axi-symmetric elements were used to model the cylinder and a constant average CTE for each layer was determined by a rule of mixtures method. The residual stresses generated due to mismatch in CTEs at the interfaces between adjacent layers were determined. The results show the residual stresses generated due to the CTE mismatch between the adjacent layers. It should be noted that the elastic mismatch between adjacent layers was small, so the elastic constants were assumed to be the same in all layers. The cylinder is free from external stresses so no boundary restraints are applied in the FE analysis. Fig. 4a-b show that the significant stresses (both radial and hoop directions) developed in the vicinity of the interfaces away from the surface diminish quite rapidly away from them. As expected, the results show no significant longitudinal stresses since the cylinder is free to contract along its axis. A maximum mean stress of about 115MPa is seen close to the axis of the cylinder (Fig. 4c-d). The mean stresses closer to the surface of the cylinder have a lower magnitude than those a small distance below the surface or near the centre (Fig.4d). Near the surface the total change in stress for each layer is 34 \pm 2MPa, which is close to the experimental result for the surface stress obtained from fluorescence microscopy (32MPa). Comparing Fig. 3 and Fig. 4d it is apparent that the residual stress measurements obtained from fluorescence microscopy at the surface are

consistent with both the microstresses and surface FGM stresses predicted by the appropriate models.

In summary, we have investigated an alumina-silicon carbide functionally-graded assembly with systematically varied composition. Microstructural characterisation of the structure reveals defect- and crack-free interfaces, apart from the 80-90% SiC interface where some residual porosity is evident. Finite element and analytical microstress models are consistent with surface stresses measured by Cr³⁺ fluorescence microscopy.

The authors gratefully acknowledge funding and assistance from TWI (Granta Park, Abington, Cambridge, UK).

- [1] N. Calis, S.R. Kushan, F. Kara, H. Mandal, J. Euro. Ceram. Soc. 24 (2004) 3387.
- [2] J.A. Fernie, P.L. Threadgill, M.N. Watson, Weld. Met. Fabr. 59 (1991) 179.
- [3] C.S. Lee, S.H. Ahn, L.C. DeJonghe, G. Thomas Mat. Sci. Eng. A 434 (2006) 160.
- [4] J.F. Shackelford and W. Alexander (Eds.), CRC Materials Science and Engineering Handbook, CRC Press, Boca Raton, USA, 2001.
- [5] C. Kawai, S. Wakamatsu J. Mater. Sci. Lett. 14 (1995) 467.
- [6] C.S. Lee, X.F. Zhang, G. Thomas Acta Materialia 49 (2001) 3775.
- [7] M. Ito, N. Ishida US Patent No. 4723862 (1988)
- [8] D. Sciti, A. Bellosi J. Mater. Sci. 35 (2000) 3849.
- [9] T. Kinoshita, S. Munekawa, S. Tanaka Acta Materialia 45 (1997) 801.
- [10] J.A. Coppola, N. Hailey, C.H. McMurty US Patent No. 4346049 (1982).
- [11] J.J. Kim J. Mater. Sci. Lett. 15 (1996) 1754.
- [12] F. K. van Dijen, E. Mayer J. Euro. Ceram. Soc. 16 (1996) 413.
- [13] R.L. Coble US Patent No. 3026210 (1962).
- [14] S.I. Bae, S. Baik J. Mater. Sci. 28 (1993) 4197.
- [15] M.N. Rahaman Sintering of Ceramics CRC Press, Boca Raton, USA, 2008.
- [16] W. Jo, D.Y. Kim, N.M. Hwang J. Am. Ceram. Soc. 89 (2006) 2369.
- [17] J.L. Ortiz-Merino, R.I. Todd Acta Materialia 53 (2005) 3345.
- [18] Niihara, K J. Ceram. Soc. Jpn. 99 (1991) 974-982.
- [19] J.L. Ortiz-Merino, R.I. Todd J. Eur. Ceram. Soc. 23 (2003) 1779.
- [20] R.I. Todd, B. Derby Acta Materialia 52 (2004) 1621
- [21] A.M. Cock, I.P. Shapiro, R.I. Todd, S.G. Roberts J. Am. Ceram. Soc. 88 (2005) 2354.
- [22] Q.Z. Yang, T. Troczynski J. Am. Ceram. Soc. 83 (2000) 958.
- [23] E.M. Levin, C.R. Robbins, H.F. McMurdie, Phase diagrams for ceramists American Ceramic Society, Columbus, Ohio, 1969.
- [24] M. Herrmann, R. Neher, K. Brandt, S Hoehn J. Euro. Ceram. Soc 30 (2010) 1495.
- [25] Q. Ma, D.R. Clarke J. Am. Ceram. Soc. 76 (2005) 1433.
- [26] J. He, D.R. Clarke J. Am. Ceram. Soc. 78 (1995) 1347.
- [27] R.I. Todd, M.A.M. Bourke, C.E. Borsa, R.J. Brook Acta Materialia 45 (1997) 1791.
- [28] R.I. Todd, A.R. Boccaccini, R. Sinclair, R.B. Yaltee, R.J. Young Acta Mater. 47 (1999) 3233.

1
2
3
4
5
6
7
8
9
10
11
12
13
14
15
16
17
18
19
20
21
22
23
24
25
26
27
28
29
30
31
32
33
34
35
36
37
38
39
40
41
42
43
44
45
46
47
48
49
50
51
52
53
54
55
56
57
58
59
60
61
62
63
64
65

Figure 1: As-sintered FGM cylinder and polished cross-section showing layered structure.

Figure 2: Back-scattered scanning electron microscope images of regions of interest a) alumina-rich end b) centre of the FGM c) interface between 80%-90% SiC layers d) SiC-rich end.

Figure 3: Model for interphase stresses and experimental data for Cr^{3+} fluorescence R1 peak position as function of distance along the FGM from the alumina-rich end.

Figure 4: Finite element modelling of residual stresses in a FGM cylinder. a) Radial stress b) hoop stress, c) mean stress, d) line-scan of mean stress along the longitudinal axis of the cylinder at positions ~ 0.2 mm (“Surface”) and ~ 0.8 mm (“Sub-Surface”) from the outer surface, and at the central axis of the cylinder (“Centre”).

